Picosecond photoelectron microscope for high-speed testing of integrated circuits

by P. May Y. Pastol J.-M. Halbout G. Chiu

The performance of devices and circuits is advancing at a rapid pace with the advent of submicron design ground rules and switching times under 50 ps. The requirements for probing the internal nodes of these ultra-fast, -small, and -dense circuits give rise to great challenges for high-speed electron-beam testing. In this paper, we review the steps which have allowed electron-beam testing to achieve simultaneously 5-ps temporal resolution, 0.1- μ m spot size, and 3 mV/ $\sqrt{\text{Hz}}$ voltage sensitivity. The resulting newly developed instrument, called the picosecond photoelectron scanning electron microscope (PPSEM), is capable of measuring the state-of-the-art bipolar and FET circuits and also VLSI passive interconnects.

[®]Copyright 1990 by International Business Machines Corporation. Copying in printed form for private use is permitted without payment of royalty provided that (1) each reproduction is done without alteration and (2) the *Journal* reference and IBM copyright notice are included on the first page. The title and abstract, but no other portions, of this paper may be copied or distributed royalty free without further permission by computer-based and other information-service systems. Permission to *republish* any other portion of this paper must be obtained from the Editor.

1. Introduction

Constant progress in lithography, innovations in device structures, and better understanding of scaling laws are pushing the speed and density of integrated circuits at a relentless pace. The fastest bipolar nonthreshold logic (NTL) and emitter-coupled logic (ECL) operate with gate delays of 25.8 ps [1] and 38.8 ps [2], respectively. Silicon NMOS circuits with $0.1-\mu m$ gate length have recently achieved a 13.1-ps [3] gate delay. To characterize the performance of these high-speed circuits, the time resolution of the measuring instrument for rise-time/falltime measurements must be well under the 10-ps mark, and the intrinsic jitter of this instrument must be kept in the 1-2-ps region. In addition to the stringent speed requirements, it is of paramount importance for internal node probing to retain a high spatial resolution (0.1 µm), both for the probe size and for its placement in order to locate and probe the node of interest successfully.

Mechanical probes are inadequate for submicron technologies, and contactless probing techniques are essential to the rapid development of these advanced circuits. Recent efforts using laser techniques for waveform measurements have demonstrated sufficient temporal resolution [4–7], but they are unlikely to provide easily the submicron resolution required for

probing digital LSI and VLSI circuits. Scanning electron microscopes (SEM) offer a spot size that neither optical techniques nor mechanical needle probes can approach. It is therefore essential to extend the already well-established electron-beam probing technology into the picosecond regime. We review in this paper the steps which have led to the development of an ultrafast electron-beam prober which takes advantage of picosecond laser technology to achieve unprecedented time resolution.

2. Conventional voltage-contrast techniques

• Quantitative voltage contrast

The basic principle of voltage contrast [8] is quite straightforward. The primary electron beam of a conventional scanning electron microscope is focused onto a conductor of the device under test. Secondary electrons (SEs), generated from the point addressed by the primary beam, have a characteristic energy distribution, dependent on the material, extending from 0 eV to 50 eV with a peak around 5 eV. The voltage on the conductor is then measured from the energy shift of this SE energy distribution, which is analyzed by an electron energy spectrometer [9].

Since the angular dependence of the collected SE signal can be misinterpreted as a voltage contrast, it is preferable to use a spectrometer design which minimizes the potential for such errors. Hemispherical analyzing grids [10] or suitably arranged magnetic collecting fields have been shown to be less sensitive to these problems [11, 12]. In addition, the spectrometer usually contains an extraction grid located as near as possible to the device under test (DUT), which helps in reducing the influence of on-chip local fields. For high-speed measurements, this extraction grid is essential in minimizing the dynamic local field effect which arises from the finite transit time of the SEs through the local field of the line under test [13]. Several automatic feedback schemes have been devised to increase the linearity range of the spectrometer and make it immune to changes in the shape of the SE spectrum which can arise from contamination or diversity of materials. Voltage sensitivities in the millivolt range have been demonstrated, although absolute dc voltage measurements usually require careful calibration [14, 15].

• Stroboscopic voltage contrast

Plows and Nixon [16] have shown that high-frequency waveforms, exceeding the intrinsic bandwidth of the SE detector, can be observed and measured using a stroboscopic voltage-contrast technique analogous to a light stroboscope. In this mode the primary beam is pulsed by a beam blanker synchronous with the repetitive waveform. Since the primary electrons only strike the

DUT at a particular phase in a given cycle, the resulting time-integrated SE current is a sample of the voltage at this particular phase of the cycle.

A conventional beam blanker comprises a parallelplate capacitor which is pulsed by a programmable pulse generator synchronized to the DUT [17, 18]. Commercial electron-beam testers have achieved a 100-ps rise-time/fall-time resolution with as little as 10 ps jitter [19], and a 7-ps time resolution was recently demonstrated in an experimental setup [20]. Although high-speed electrostatic deflectors are commonly used for beam blanking, they present several practical difficulties: 1) It is a challenge to efficiently generate picosecond electron pulses of large enough amplitude. 2) To avoid device damage and charging effects, the primary-beam energy is kept in the range 0.5-2 keV for testing applications; this variable low-beam energy complicates the design of the beam blanker. 3) The deflection system can degrade the probe spot size [11] on the DUT unless the electron optics are carefully designed to accommodate this moving object. 4) Impedance matching between the blanker and its driver must be achieved over a wide bandwidth.

The first of these challenges is the most critical when submicron spatial resolutions and picosecond temporal resolutions are required. In an SEM, the primary-beam current is a function of the spot size [21]; at a given brightness, a smaller spot implies a smaller amount of current reaching the DUT, and therefore a deterioration of the signal-to-noise ratio, as the SE signal is directly proportional to the primary-beam current. These conflicting requirements result in a compromise between the spot size and beam current. For testing of integrated circuits (IC) with features between 1–3 μ m, a spot size of 0.3-1 µm is used, with a resulting beam current of the order of 1-10 nA with a conventional LaB, SEM gun. (Note that thermal field emitter systems with higher currents are just becoming commercially available.) A smaller spot size down to $0.1-0.3 \mu m$ is required in the submicron regime, with a concurrent reduction in beam current. This results in a poorer signal-to-noise ratio for voltage-contrast measurements, or longer measurement times as the device size shrinks. In the case of high-speed voltage-contrast stroboscopic sampling, the beam current is further reduced by the duty cycle. A small beam current implies impractically long measurement timemany hours for 5-10-ps resolution. For this reason, it is important to develop a high-brightness gun in order to keep the waveform measurement time to an acceptable level (seconds to minutes). This brightness problem and the other complications previously mentioned are avoided with the picosecond photoelectron SEM described below, where the source itself is modulated to produce the sharp probe pulses.

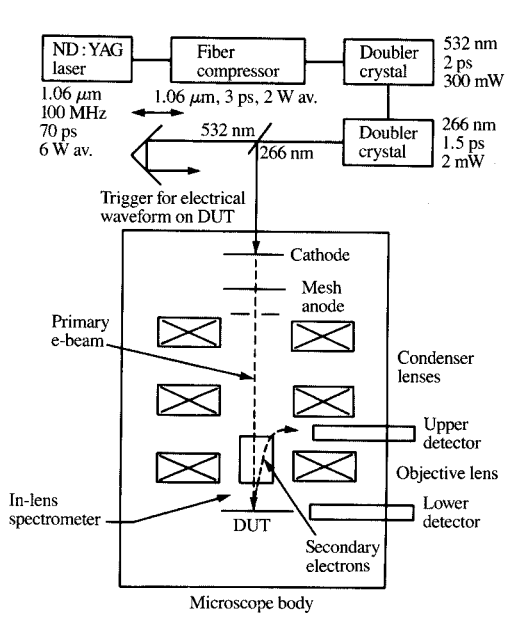


Figure 1 Schematic of the picosecond photoelectron scanning electron microscope.

The fast waveform measurements are carried out through sampling and signal averaging in order to reconstruct the waveform with a good signal-to-noise ratio [22]. In the sampling mode, repetitive waveforms must be applied to the DUT. However, a particular internal node of a complex circuit may or may not toggle at every clock cycle. Therefore, the test time, in the sampling case, is lengthened to the product of the sampling time and the repetition period of the node under test. Further in-depth reviews of conventional high-speed e-beam probing can be found in [23] and [24].

3. Picosecond photoelectron SEM

The rapid advances in ultrashort optical pulses have given optical techniques a comfortable edge with respect to time resolution. Taking advantage of these advances, a novel instrument called the picosecond photoelectron scanning electron microscope (PPSEM) [25, 26] was recently developed which combines the high temporal resolution of the laser techniques and the high spatial resolution of the SEM. This instrument also provides solutions to the problems inherent in ultrafast e-beam probing which were previously discussed.

• Description of the instrument

In this new instrument, the thermionic electron gun of a conventional SEM is replaced by a pulsed laser/photocathode combination. **Figure 1** shows a schematic of the system. The laser source consists of a mode-locked Nd:YAG laser which produces 70-ps pulses at $1.06~\mu m$ and at a repetition rate of 100 MHz. The laser pulses are compressed in a fiber-grating optical pulse compressor to less than 3 ps full width at half maximum (FWHM). The compressed pulses are then frequency-doubled to 532 nm in a potassium titanyl phosphate (KTP) crystal, resulting in 2-ps pulses of 532 nm (green) with an average power in excess of 300 mW. Subsequent frequency doubling in a potassium dihydrogen phosphate (KDP) crystal yields over 2 mW of average ultraviolet (uv) power at 266 nm with pulses of only 1.5-ps duration.

The uv light thus produced is focused onto a photocathode mounted at the head of the SEM column. The photocathode consists of a roughened gold film of 200 Å thickness evaporated onto a fused quartz substrate, and it is used in transmission with the light focused through the transparent substrate. The photoelectrons are produced by single-photon photoemission. With an average optical input power of 2 mW and with a typical conversion efficiency of 0.2×10^{-3} , an average current of 100 nA is produced, with approximately 6000 electrons in a 1.5-ps pulse. For a spot size at the cathode of 4 μ m, and assuming a semi-angle of divergence for the electron beam of 3×10^{-3} rad (with the photon energy just at the work function, the excess photoelectron energy is of order 25 meV), the peak brightness of this photocathode is 3×10^8 A/cm² steradian at a beam energy of 1.8 keV. Let us point out here that this brightness is comparable to the field emission regime [21, 27] without, however, the ultrahigh vacuum requirements.

Since the spot size on the photocathode is relatively small (that is, less than the diameter of the beam at its crossover point in a thermionic SEM), it can be used directly as the object for the electron optics without the need for a Wehnelt electrode. In most cases, an average cathode current of 1 nA is sufficient to see real-time-scanned images of the DUT. This feature is essential for subsequent positioning of the electron probe onto the node of the circuit where the voltage is to be measured.

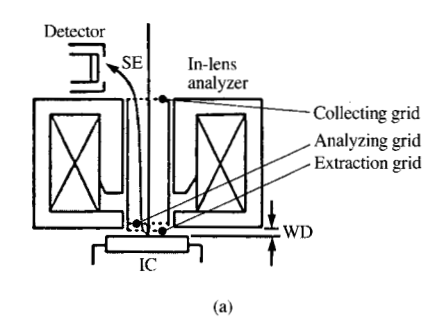
Typical operating conditions use a cathode current of 10 nA. The gold cathodes show no deterioration in efficiency through exposure to atmosphere. The gun vacuum is typically only 10⁻⁵ torr during operation. A high extraction field at the photocathode minimizes any pulse broadening due to Coulomb interactions and also raises the threshold for the onset of space-charge effects [28]. This can be accomplished either with a mesh or with an aperture in close proximity to the cathode, or by reducing the cathode-anode spacing. Operation occurs at

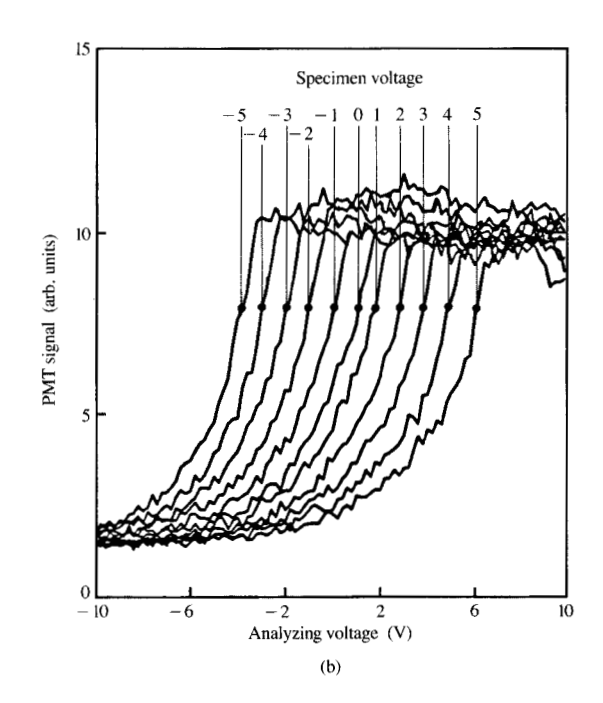
accelerating fields between 1 and 1.5 kV/mm. Most of the voltage drop occurs between the cathode and extraction mesh when such a configuration is used. Measurements show that the emitted photocurrent follows the input uv average power linearly, which confirms that photoemission is not in the space-charge-limited region. The primary-electron beam is then focused onto the conductors of the DUT using a conventional SEM.

For voltage measurements, an in-lens analyzing spectrometer was implemented based on a simplified three-grid Feuerbaum design [14, 15] shown in Figure 2(a). The secondary electrons are accelerated by an extraction grid with a potential of typically 2 keV about 1 mm from the sample. They are subsequently analyzed by an analyzing grid typically at a few volts potential. This grid acts as a high-pass filter—only secondary electrons with sufficient energy pass through it and are attracted to the collector grid (typically at a few volts) and then to the scintillator/photomultiplier tube combination, where a current proportional to the number of analyzed secondaries is produced. The signal produced for different specimen voltages as the voltage on the analyzing grid is scanned is shown in Figure 2(b). For waveform measurements there are three primary modes of operation [26]. For small swings of specimen voltage (i.e., small-amplitude waveforms less than 2 volts), the analyzing voltage is judiciously chosen and fixed such that the measured photomultiplier tube current is linear with specimen voltage—this region can be discerned from the figure. Alternatively, the analyzing voltage is changed with the specimen voltage to keep the photomultiplier current constant, and the specimen voltage is then directly related to the analyzer voltage. Even more effective is to use a feedback loop to keep the photomultiplier current signal at the inflection point of the curves shown in the figure. The specimen voltage is again related directly to the analyzer voltage, but now the measurement is insensitive to changes in the total yield of secondary electrons. These last two techniques are particularly important when measuring large voltage swings.

• Temporal resolution

The characterization of the time-resolution capabilities of this instrument was carried out by measurement of well-defined electrical signals with picosecond rise-times. To this effect, pulses photoconductively launched on 2.4-µm coplanar aluminum transmission lines fabricated on an epitaxial layer of silicon on a sapphire substrate were measured [29]. The fast photoconductor can generate a voltage step with a 2-ps rise-time (i.e., determined by the light pulse duration) and a long fall lasting over 200 ps, with a peak amplitude of about 50 mV. Figure 3 shows

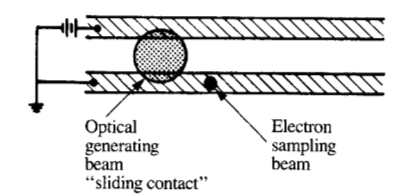




(a) Three-grid planar retarding field analyzer with (b) corresponding "S" curves.

the measured SE signal when the primary beam is focused at three successive points along the grounded wire of the transmission line pair. Here the extraction field is set at 1 kV/mm. The primary-electron-beam energy is 1.8 keV for these measurements with an accelerating field at the photocathode of 1 kV/mm.

The rise-time measured at the generation site of the electrical pulse is under 6 ps, which, with an actual pulse rise-time of 2 ps, gives an instrumental resolution of about 5 ps. With a spectrometer extraction field of 2 kV/mm, measured rise-times were under 5 ps, leading to an instrumental resolution of 4 ps for these fields and geometries. According to Monte Carlo simulations [26],



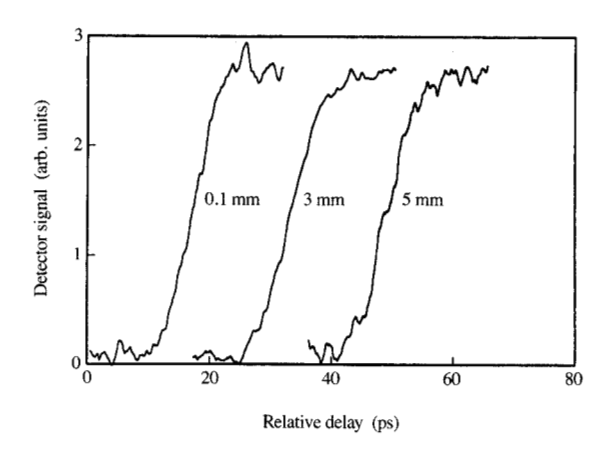


Figure 3

(a) Sliding-contact mode of photoconductive excitation on a coplanar pair transmission line and (b) measured waveforms generated by sliding-contact excitation on 2.4- μ m coplanar lines with 4.8- μ m separation. The waveforms are measured at the indicated distances from the point of generation.

this temporal resolution is determined primarily by the transit time of the SEs through the time-varying local fields of the lines [30]. Note that the intrinsic dispersion of the transmission line is very small and is reflected in the rounding of the waveform rising edge, which the instrument displays very well.

Jitter and sampling

Conventional stroboscopic electron-beam testers have jitters between 10 and 50 ps [19]. For the measurements presented here, the phase delay between the waveform to be measured and the probe electron pulse is implemented by varying the optical paths of these two arms. This approach has the advantage of an extremely low jitter, well under 1 ps. Alternatively, it has been shown that this phase delay can also be generated electronically by offset of the triggering frequency with respect to the probing frequency [31]. For this, the mode-locked laser optical pulse train is slaved to a master clock with subpicosecond phase noise [32]. This approach is obviously less

cumbersome and easier to implement in a fully integrated system.

Though the sampling rate of this instrument is restricted to the laser repetition rate (or, by pulse picking, a subharmonic), the DUT can be driven at multiples of the laser frequency into the GHz clocking regime, as long as the phase of this clock is well controlled with respect to the sampling probe train.

• Spatial resolution

A crucial characteristic of the microscope for waveform measurements on circuits is its spatial resolution, in terms of both the spot size and the ability to repeatedly position it accurately. These latter characteristics are a standard feature of any SEM achieved through the deflection coils positioned above the objective lens. However, the probe size must also be characterized at the operating conditions of the instrument. A knife-edge technique was used for this measurement. For this, the cleaved edge of a GaAs wafer is positioned to mask part of the opening of a Faraday cup. SEs are collected as the beam scans over the GaAs but not when it strikes into the Faraday cup. From the magnification of the scan, it is then possible to deduce the probe size, defined as the FWHM of the electron spatial distribution. At the same time, the probe current can be measured from a picoammeter connected to the otherwise isolated Faraday cup. For a typical cathode current of 10 nA, an optical spot size at the cathode of 10 μ m, and a primary-electron energy of 1.8 keV, the beam current at the sample is about 50 pA, with a probe size of 0.1 μ m. Further optimization of the optical and electron-optical lens systems should allow for smaller probe sizes and possibly higher probe currents. In particular, tighter focusing at the cathode to give a smaller laser spot size should give a commensurate decrease in the electron probe diameter. The present performance compares most favorably with the spatial resolution of conventional SEM at comparable beam energies and working distances. Such performance emphasizes that the photoelectron source is indeed very bright, with an energy spread much less than 1 eV. Since the beam is naturally pulsed, the need for a beam blanker, with its associated difficulties, is avoided.

• Voltage resolution

For waveform measurements, the voltage resolution of the instrument is of prime importance. The instrument operates in a stroboscopic mode, where the voltage at one given point on the waveform is measured by signal averaging, and the measurement time is therefore dependent on the desired voltage sensitivity. To reduce the influence of the laser AM noise, the device trigger beam is modulated at 100 kHz by an acousto-optic modulator, and the signal is recovered by a lock-in

amplifier at the output of the secondary-electron detector. A sevenfold increase in the voltage sensitivity is observed upon increasing the chopping frequency from 3 kHz to 100 kHz. At this latter modulation frequency, a voltage sensitivity better than 3 mV/ $\sqrt{\text{Hz}}$ was measured, where a signal-to-noise ratio of 2:1 is regarded as detectable. In a typical mode of operation with a photocurrent of 10 nA at the cathode and 50 pA at the sample with a duty cycle of 10^{-4} , this sensitivity is within a factor of 2 of the shotnoise limit. At this sample current, the conductors on the DUT are being probed with three to five electrons per pulse, compared with, on average, a fraction of an electron per pulse in conventional beam-blanked systems.

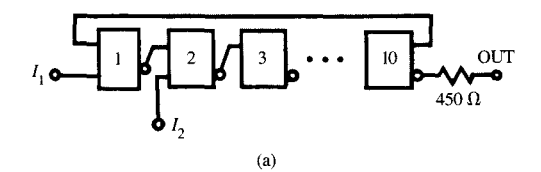
Furthermore, the loading of this probe is truly negligible. Since the primary-beam energy is chosen close to the second crossover point of the SE yield, there is no net charge injected into the DUT. Actual circuit measurements have shown no influence of the primary beam on the operation of the circuits, and no damage was ever detected for either small-dimension CMOS devices or silicon bipolar circuits.

4. Measurements on circuits

circuits.

• High-performance silicon bipolar circuits The first example of application of this tool is waveform measurements at the internal nodes of a sub-100-ps emitter-coupled logic (ECL) bipolar ring oscillator [33]. For these measurements, the circuit self-oscillation is disabled and a trigger is supplied from a photodiode. Figure 4 shows a schematic of the ring oscillator made up of ten ECL gates together with the circuit layout of an individual gate. I_{i} is a disabling input (to prevent oscillation) and I_2 , the external pulse input. Thus, in the configuration used here, the circuits act as a chain of ECL gates with a fan-in and a fan-out of unity. The waveforms can be measured at any point within the circuit, e.g., at the terminals of the component transistors, thereby providing a detailed account of its internal operation. These measurements represent the first time that such internal waveforms have been measured and fully characterized on high-speed silicon

Figure 5 shows a typical set of waveforms measured at the input of a gate, the output of its current switch (waveform B), and the output of its emitter-follower stage (waveform A), but for two gate types, i.e., an unloaded gate (representative of gates 1–9) and a loaded gate (gate 10 with feedback loop to gate 1). For the unloaded gate, the total measured gate delay of 90 ps and the rise-times of 150 ps obviously do not stretch the capability of the instrument. The measured 12-ps delay through the emitter-follower can already be seen in these data and was ascertained from higher-resolution scans. We can



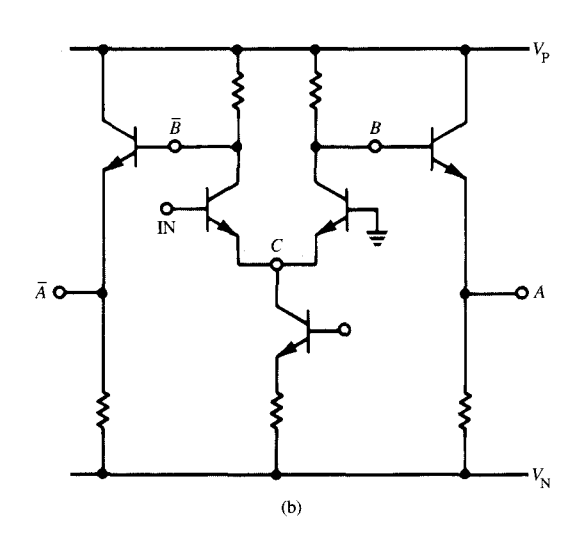
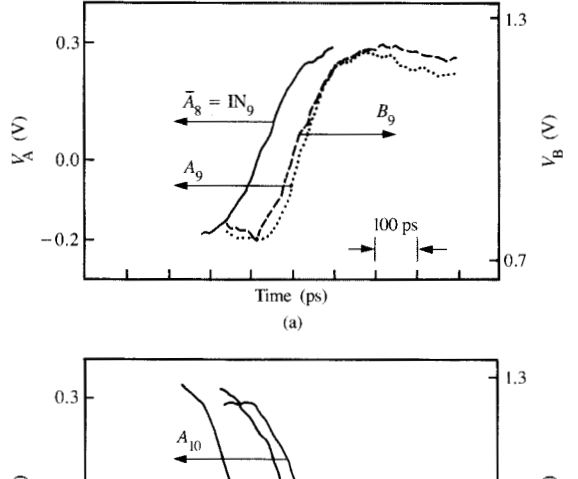


Figure 4

(a) Schematic of the ring oscillator and (b) detail of a single ECL gate.

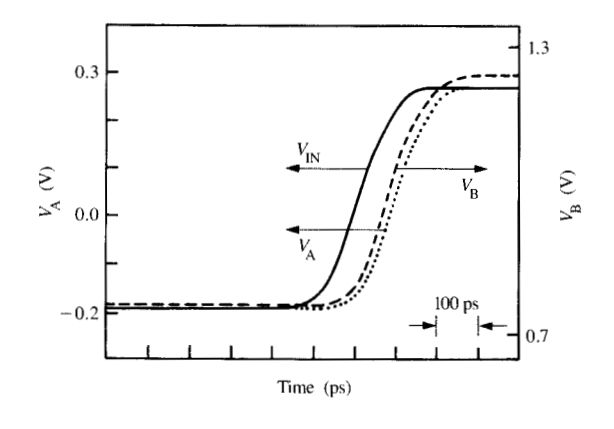
also clearly see the effect of loading, with the total delay through gate 10 being 160 ps with the emitter-follower contribution itself increased to 35 ps. The increase in delay through the current switch with respect to the unloaded stages indicates that the emitter-follower does not completely isolate the capacitive load. Typical acquisition times for these waveforms were about 15 s, with 1000 data points per waveform stored into the controlling personal computer.

Besides the influence of loading, changes in voltage swing and power consumption can be studied in detail on an individual gate, in situ, and compared to circuit models and to data from other gates. This provides an essential control on the device fabrication process, its influence on the high-speed performance of the circuit, and the aptitude of the model to reflect the fabricated circuits. Figure 6 shows a model for the internal gate delays for an unloaded gate and can be compared with the data in Figure 4. Another unique measurement that can be made on these circuits with the PPSEM is a comparison of gate switch-on versus switch-off (see



a fathlight

Waveforms measured at three different points inside the gate for both (a) unloaded gate (gate 9) and (b) loaded gate (gate 10).



Model-derived waveforms for gate 9.

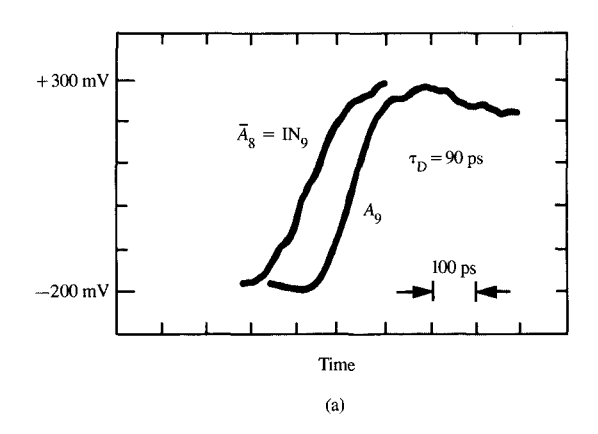
Figure 7). Turn-on of the gate occurs through passive charging of the node B through a resistor, as compared to the active discharge of turn-off through the reference transistor, and thus turn-on is slower than turn-off (90 ps vs. 80 ps).

◆ CMOS SRAM measurements

As a second example, we present room-temperature and low-temperature (80 K) measurements of the access time of a 0.5-\mu CMOS SRAM [34] from the clock input to the cell, and its breakdown into individual delays between logic devices (inverters, NOR and NAND gates) in the prelogic leading to the selected cell. The circuit was fabricated in a 0.5-µm selectively scaled CMOS technology. The smallest dimension at the metal level was 1.2-μm line width with 1.0-μm contacts. The insulation between the first and second metal wiring layers was etched away so that both metal layers were accessible for e-beam measurements. To synchronize the measured waveforms to the pulsed electron probe, a photodiode was used to provide the trigger to a pulse generator that in turn supplied a 100-MHz square-wave signal (3.3-V amplitude) to the clock pad on the chip. A particular memory cell in this experimental 576-bit SRAM was selected by supplying appropriate static address voltages. The chip was mounted in a 40-pin dip package and placed on the x-y stage of the PPSEM. The package can be cooled to 80 K (measured with a diode) by a liquid nitrogen flow, permitting low-temperature measurements. The logic path from the clock input to the cell is shown in Figure 8(a), where the measurement points are identified by numbers. Figure 8(b) shows the measured room-temperature and low-temperature measured waveforms. The overall access time to the cell is 1400 ps at room temperature, and 1110 ps at 80 K. With the high temporal resolution of the apparatus, it is possible to characterize each logic gate in terms of risetime/fall-time and gate delay, and to accurately determine how these characteristics are modified at low temperature.

• 0.25-µm-gate-length inverter chain

Finally, inverter chains fabricated in a 0.25-µm-gate-length silicon NMOS technology [3] were also investigated at room temperature. The circuits were externally triggered by a photodiode-pulse generator combination, as described above. The measurements were performed by directing the pulsed electron probe on the 0.25-µm-wide lines interconnecting the successive stages of the chain. The corresponding results are displayed in **Figure 9** for the output of four consecutive inverters in the chain. An average gate delay of 23 ps and rise-times/fall-times of 25 ps were observed for room-temperature operation. These measurements clearly



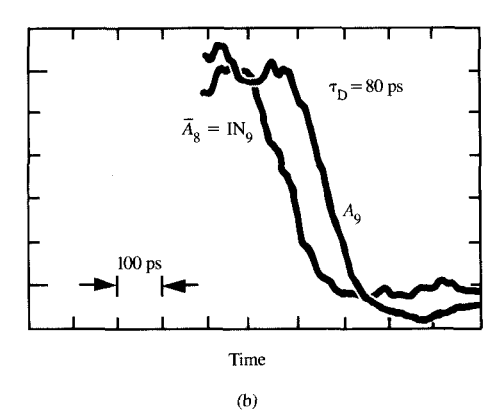


Figure 7

Switch-on (a) versus switch-off (b) delay for gate 9.

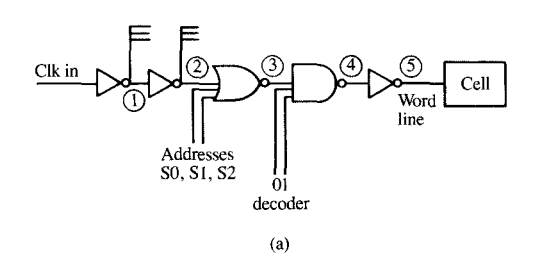
demonstrate the simultaneous temporal and spatial resolutions of the PPSEM.

5. Passive interconnect measurements

• Thin-film package

Aside from measuring delays and rise-times and falltimes from active devices, the PPSEM also has the potential to characterize passive interconnect structures. One such measurement has already been discussed in Section 3 in the context of measuring the temporal resolution of the instrument. Minimal dispersion of 5-ps rise-time pulses was observed over 5-mm propagation on a coplanar transmission line. Here measurements on an experimental interconnection structure fabricated with a thin-film technology are presented [35]. The sample under investigation consisted of a series of 8-µm-wide and 5.35-\(\mu\)m-thick copper microstrip transmission lines separated from a uniform ground plane by a 6.5-µmthick layer of polyimide. The lines were embedded in the polyimide with their top surface exposed. The pitch of the lines was 25 μ m. A step-recovery diode was triggered in synchronism with the laser pulse train to produce approximately 100-ps-wide electrical pulses which were then electrically launched onto this thin-film sample with a short length of high-speed coaxial cable.

Measurements were made at the beginning and also at several points along the length of the line (Figure 10). The first peak in the waveforms corresponds to the input pulse traveling past the measurement point, and the second peak corresponds to the same pulse reflected back



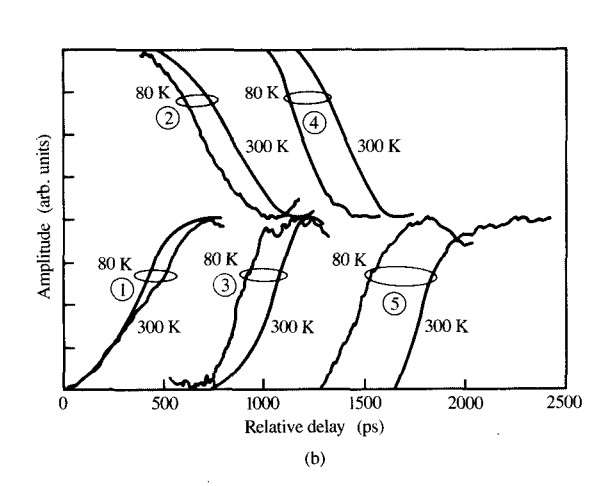
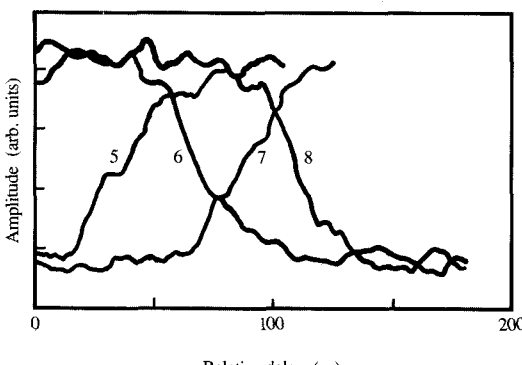


Figure 8

(a) Schematic for the device path in the pre-logic leading to a cell in the 0.5- μm CMOS SRAM and (b) corresponding waveforms. The dc levels have been shifted and the amplitudes have been renormalized for ease of comparison. Waveforms measured at both room temperature and $80 \, \text{K}$ are shown.



Relative delay (ps)
(a)

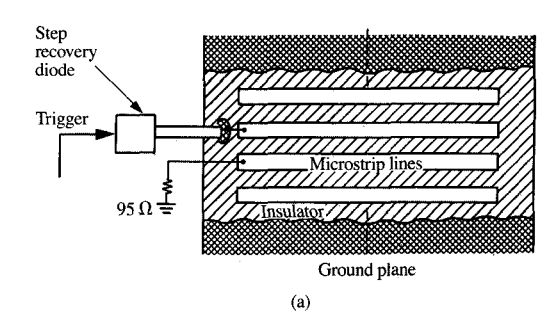
D G

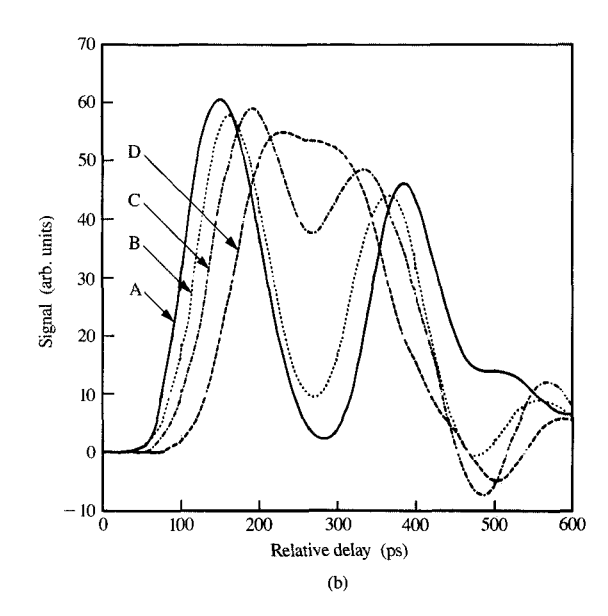
Stantis 6

(a) Output waveforms of the successive stages of a 0.25- μ m NMOS inverter chain and (b) photograph of a single cell. The upper transistor in the cell is used as a load. The drain from this cell connects to the gate of the succeeding cell. The 0.25- μ m-wide line that served as the measuring node is indicated.

from the end of a 25-mm-long open-circuited line. Consequently, the delay and distortion of the

SUKA





Floure 10

(a) Schematic of the experimental thin-film interconnection structure and (b) waveforms measured at various points along a thin-film microstrip transmission line: Curve A, 0 mm; Curve B, 5 mm; Curve C, 10 mm; Curve D, 15 mm.

transmission line can be deduced by comparison of the two peaks in each waveform. The contactless probing capabilities of the electron beam permit the positioning of the probe point at any point where the waveform needs to be studied.

• Circuit interconnect

As active devices become faster, it is increasingly the interconnect delays that determine the operation speed in computer systems. This delay is not only determined by off-chip interconnects, but can also become significant in intra-chip connections. In Section 4, active device measurements on a 0.5- μ m CMOS SRAM were discussed. There was a 500- μ m interconnect between the output of the second inverter and the input to the NOR

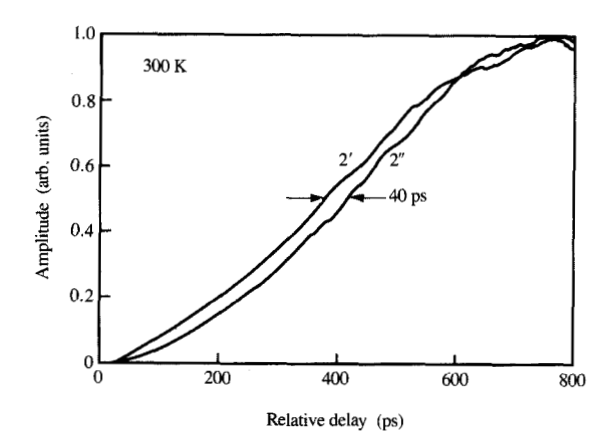
gate, and measurements were made at the extremities of the lines. Figure 11 shows the result: At room temperature, a 40-ps on-chip delay was measured. This is, to the best of our knowledge, the first accurate measurement of an on-chip wiring delay. The interconnect approximates to a microstrip line, and the effective index of the substrate to account for such a delay would have to be about 25, i.e., about seven times larger than one would expect from the index of silicon. This effective index increase is caused by the slow-wave effect; for the given dimensions of the line, the resistivity of the substrate, and the pulse duration, the effective index measured here agrees with theory [36].

6. Summary

We have reviewed in this paper the recent evolution of high-speed electron-beam probing of VLSI internal nodes. The advent of the PPSEM technology makes the future of electron-beam probing very promising by allowing it to stay abreast of progress in device technology. The simultaneous characteristics of the PPSEM for stroboscopic voltage-contrast measurements are unique, with a temporal resolution of better than 5 ps, a voltage resolution of less than 3 mV/ $\sqrt{\text{Hz}}$, and a probe size of 0.1 µm for a cathode current of 10 nA and a sample current of 50 pA. Typical waveform measurement times for these parameters are of the order of 15-20 seconds. This as yet experimental instrument should develop into an extremely valuable tool for highperformance circuit development and fault analysis. This will, however, require coupling of the e-beam prober and the design data of the circuit [37, 38] to simplify the task of the user, who will then be able to use the instrument as a simple sampling oscilloscope.

References

- T. Sakai, S. Konaka, Y. Yamamoto, and M. Suzuki, "Prospects of SST Technology for High Speed LSI," *IEDM Tech. Digest*, p. 18 (1985).
- J. Warnock, P.-F. Lu, T.-C. Chen, K. Y. Toh, J. D. Cressler, K. A. Jenkins, D. D. Tang, J. Burghartz, J. Y. C. Sun, C. T. Chuang, G. P. Li, and T. H. Ning, "A 27 GHz 20 ps PNP Technology," *IEDM Tech. Digest*, p. 903 (1989).
- G. A. Sai-Halasz, M. R. Wordeman, D. P. Kern, E. Ganin, S. Rishton, H. Y. Ng, D. S. Zicherman, D. Moy, T. H. P. Chang, and R. H. Dennard, "Inverter Performance of Deep Submicron MOSFETS," *IEEE Electron Device Lett.* 9, 633 (1988).
- B. H. Kolner and D. M. Bloom, "Electrooptic Sampling in GaAs Integrated Circuits," *IEEE J. Quantum Electron.* QE-22, 79 (1986).
- J. A. Valdmanis and G. Mourou, "Sub-picosecond Electrooptic Sampling: Principles and Applications," *IEEE J. Quantum Electron.* QE-22, 69 (1986).
- R. B. Marcus, A. M. Weiner, J. H. Abeles, and P. S. D. Lin, "High-Speed Electrical Sampling by Femtosecond Photoemission," Appl. Phys. Lett. 49, 357 (1986).
- H. K. Heinrich, D. M. Bloom, and B. R. Hemenway, "Noninvasive Sheet Charge Density Probe for Integrated Silicon Devices," Appl. Phys. Lett. 48, 1066 (1986).



a amenda

On-chip propagation delay measured between the two extremities of a 500-µm-long interconnection line.

- C. W. Oatley and T. E. Everhart, "Examination of p-n Junctions with the Scanning Electron Microscope," *J. Electron.* 2, 568 (1957).
- O. C. Wells and C. G. Bremer, "Voltage Measurement in the Scanning Electron Microscope," J. Phys. E: Sci. Instrum. 1, 902 (1968)
- Y. Goto, A. Ito, Y. Furukawa, and T. Inagaki, "Hemispherical Retarding Type Energy Analyzer for IC Testing by Electron Beam," J. Vac. Sci. Technol. 19, 1030 (1981).
- S. C. J. Garth, W. C. Nixon, and D. F. Spicer, "Magnetic Field Extraction of Secondary Electrons for Accurate IC Voltage Measurement," J. Vac. Sci. Technol. B 4, 217 (1986).
- N. Richardson and A. Muray, "An Improved Magnetic Collimating Secondary Electron Energy Filter for VLSI Diagnostics," J. Vac. Sci. Technol. B 6, 417 (1988).
- H. Fujioka, K. Nakamae, and K. Ura, "Analysis of the Transit Time Effect on Stroboscopic Voltage Contrast in the Scanning Electron Microscope," J. Phys. D 18, 1019 (1985).
- H. P. Feuerbaum, "VLSI Testing Using the Electron Probe," Scanning Electron Microscopy, Vol. I, Illinois Institute of Technology Research Institute, Chicago, 1979, p. 285.
- E. Menzel and E. Kubalek, "Secondary Electron Detection Systems for Quantitative Voltage Contrast Measurements," Scanning 5, 151 (1983).
- G. S. Plows and W. C. Nixon, "Stroboscopic Scanning Electron Microscopy," J. Phys. E: Sci. Instrum. 1, 595 (1968).
- H. P. Feuerbaum and J. Otto, "Beam Chopper for Subnanosecond Pulses in Scanning Electron Microscopy," J. Phys. E: Sci. Instrum. 11, 529 (1978).
- E. Menzel and E. Kubalek, "Electron Beam Chopping Systems in the SEM," Scanning Electron Microscopy, Vol. I, Illinois Institute of Technology Research Institute, Chicago, 1979, p. 305.
- H. Todokoro, S. Yoneda, S. Seitou, and S. Hosoki, "Electron Beam Tester with 10 Picosecond Time Resolution," *Proceedings* of the 1986 IEEE International Test Conference, Washington, DC, p. 600.
- D. Winkler, R. Schmitt, M. Brunner, and B. Lischke, "Flexible Picosecond Probing of Integrated Circuits with Chopped Electron Beams," IBM J. Res. Develop. 34, 189 (1990, this issue).

- L. J. Balk, H. P. Feuerbaum, E. Kubalek, and E. Menzel, "Quantitative Voltage Contrast at High Frequencies in the SEM," Scanning Electron Microscopy, Vol. IV, Illinois Institute of Technology Research Institute, Chicago, 1976, p. 615.
- H. P. Feuerbaum, "Electron Beam Testing: Methods and Applications," Scanning 5, 14 (1983).
- E. Menzel and E. Kubalek, "Fundamentals of Electron Beam Testing of Integrated Circuits," Scanning 5, 103 (1983).
- O. C. Wells, Scanning Electron Microscopy, McGraw-Hill Book Co., Inc., New York, 1974.
- P. May, J.-M. Halbout, and G. Chiu, "Picosecond Photoelectron Scanning Electron Microscope for Noncontact Testing of Integrated Circuits," Appl. Phys. Lett. 51, 145 (1987).
- P. May, J.-M. Halbout, and G. Chiu, "Noncontact High-Speed Waveform Measurements with the Picosecond Photoelectron Scanning Electron Microscope," *IEEE J. Quantum Electron*. OE-24, 234 (1988).
- J. Orloff, "A Comparison of Electron Guns for High Speed Electron Beam Inspection," Scanning Electron Microscopy, Vol. IV, Illinois Institute of Technology Research Institute, Chicago, 1984, p. 1585.
- G. Massey, "Laser Photoelectron Sources of High Apparent Brightness," *IEEE J. Quantum Electron.* QE-20, 103 (1984).
- P. G. May, G. P. Li, J.-M. Halbout, M. B. Ketchen, C.-C. Chi, M. Scheuermann, I. N. Duling III, D. Grischkowsky, and M. Smyth, "Picosecond Electrical Pulses in Microelectronics," Conference Proceedings of Picosecond Phenomena V, G. R. Fleming and A. E. Siegman, Eds., Springer-Verlag, New York, 1986, p. 120.
- R. Clauberg, A. Blacha, and H. Beha, "Cross-Talk and Transit-Time Effects in Stroboscopic Voltage Measurements via Electron Emission," Characterization of Very High Speed Semiconductor Devices and Integrated Circuits, *Proc. SPIE* 795, 207 (1987).
- K. J. Weingarten, M. J. W. Rodwell, and D. M. Bloom, "Picosecond Sampling of GaAs Integrated Circuits," Conference Proceedings of Picosecond Electronics and Optoelectronics II, F. J. Leonberger, C. H. Lee, and H. Morkoc, Eds., Springer-Verlag, New York, 1987, p. 7.
- M. J. W. Rodwell, K. J. Weingarten, D. M. Bloom, T. Baer, and B. H. Kolner, "Reduction of Timing Fluctuations in a Mode-Locked Nd:YAG Laser by Electronic Feedback," Opt. Lett. 11, 638 (1986).
- P. May, J.-M. Halbout, C. T. Chuang, and G. P. Li, "Waveform Measurements in High Speed Silicon Bipolar Circuits Using a Picosecond Photoelectron Scanning Electron Microscope," *IEDM Tech. Digest*, p. 92 (1987).
- J.-M. Halbout, P. May, K. A. Jenkins, and G. Compeau, "SRAM Access Measurements Using a Picosecond Photoelectron Scanning Electron Microscope," ISSCC Tech. Digest, p. 82 (1988).
- G. Arjavalingam, P. May, J.-M. Halbout, and G. V. Kopcsay, "Interconnection of High Speed and High Frequency Devices and Systems," *Proc. SPIE* 947, 191 (1988).
- H. Hasegawa, M. Furukawa, and H. Yanai, "Properties of Microstrip Line on Si-SiO₂ System," *IEEE Trans. Microwave Theory & Techniques MTT-19*, 869 (1971).
- S. Concina, G. Liu, L. Lattanzi, S. Reytman, and N. Richardson, "Software Integration in a Workstation Based E-Beam Tester," *Proceedings of the 1986 IEEE International Test Conference*, Washington, DC, p. 644.
- T. Tamama and N. Kuji, "Integrating an Electron-Beam System into VLSI Fault Diagnosis," *IEEE Design & Test of Computers* 3, 23 (1986).

Received November 21, 1989; accepted for publication December 23, 1989 Paul May IBM Research Division, Thomas J. Watson Research Center, P.O. Box 218, Yorktown Heights, New York 10598. Dr. May studied natural sciences (physics) at Cambridge University, England, graduating in 1980. He received his Ph.D. in laser physics from Imperial College, London, in 1983. Since January 1986 he has been a Research Staff Member at the Thomas J. Watson Research Center. Dr. May's research interests include generation of ultrashort light pulses, time-resolved spectroscopic techniques, high-speed device characterization (optical and electron-beam techniques), and, more recently, integrated optoelectronics and chip-to-chip optical interconnects. He is a member of the American Physical Society and the Institute of Electrical and Electronics Engineers.

Yvon Pastol IBM Research Division, Thomas J. Watson Research Center, P.O. Box 218, Yorktown Heights, New York 10598. Dr. Pastol received the Ingénieur degree from the Institut Supérieur d'Electronique de Paris in 1983 and a Ph.D. in solid state physics from the University of Paris in 1987. He then joined the IBM Research Division as a Postdoctoral Fellow at the Thomas J. Watson Research Center, where he is currently involved in the development of ultrafast optoelectronic measurement techniques for materials and devices

Jean-Marc Halbout IBM Research Division, Thomas J. Watson Research Center, P.O. Box 218, Yorktown Heights, New York 10598. Dr. Halbout received the Ingénieur degree from the Institut Supérieur d'Electronique de Paris in 1977 and a Ph.D. in electrical engineering from Cornell University, Ithaca, New York, in 1981. He has been with the IBM Research Division, Thomas J. Watson Research Center, since 1983. Dr. Halbout's research interests include the applications of ultrashort optical and electrical pulses to the study of ultrafast phenomena in optical and electronic devices. Since 1983, he has been the manager of the Ultrafast Measurements Group in the Advanced Silicon Technology Department. Dr. Halbout is a member of the Optical Society of America, the Institute of Electrical and Electronics Engineers, and the Lasers and Electro-Optics Society.

George L.-T. Chiu IBM Research Division, Thomas J. Watson Research Center, P.O. Box 218, Yorktown Heights, New York 10598. Dr. Chiu received his B.S. in physics from the National Taiwan University in 1970, and the Ph.D. in astrophysics from the University of California, Berkeley, in 1978. From 1977 to 1980 he was a research staff astronomer with the Astronomy Department, Yale University, New Haven, Connecticut. In 1980 he joined the IBM Research Division, Thomas J. Watson Research Center, as a Research Staff Member. From 1980 to 1981 he worked on highspeed testing of Josephson circuits; from 1981 to 1983, he was the manager of the Josephson Circuits Group, and from 1983 to 1988 the manager of Silicon Test Systems. In the period 1988 to 1989, he served as technical staff to Dr. D. Eastman, IBM Vice President of Logic, Memory and Packaging. Since August 1989, Dr. Chiu has been the Senior Manager of Optics in the Advanced Packaging and Advanced Packaging Technology Laboratory Department. His research interests include picosecond device and internal node characterization, laser and electron-beam contactless testing techniques, functional testing of chips, optical lithography, and optoelectronics. Dr. Chiu is a member of the American Physical Society, the International Astronomical Union, and the Institute of Electrical and Electronics Engineers.